2018 4th International Conference on Systems, Computing, and Big Data (ICSCBD 2018)

A Novel Non-Metallic Ultrasonic Flaw Detection Launch System and Its Parameter Analysis

Chao Peng[1, *], Yue Song[1], Guangmin Zhang[1], Minqian Huang[1], Sha Zou[2]

[1]School of Electrical Engineering and Intelligentization, Dongguan University of Technology, Dongguan, 523808, China

[2]School of Hengnan County seventh middle, Hengyang, 421000, China

*E-mail: pengchao@dgut.edu.cn

Keywords: Ultrasonic emission system parameter analysis; Capacitive ultrasonic emission; STM32F1; Non-metallic ultrasonic flaw detection;

Abstract: In this paper, a multi-channel driving system of non-metallic ultrasonic transducer is designed.Based on the analysis of the resistance and capacitance parameters of the traditional ultrasonic transmitting circuit, this paper uses the principle that the voltage at both ends of the capacitor can not change abruptly to generate high power pulse excitation probe emission.In this paper, the field effect transistor (FET) is used as the switching control element. Compared with the traditional capacitive ultrasonic transmitting system, the whole circuit design has the advantages of multi-channel, precise and adjustable transmitting parameters, as well as other advantages such as smaller volume and larger transmitting power.he system uses STM32F1 as the main control system to output a trigger pulse signal to control the working state of the whole circuit. By establishing the circuit model of the ultrasonic transmitting circuit and making the actual circuit, it is proved that the design can generate the ultrasonic pulse excitation signal with precise adjustable frequency and amplitude.Finally, the experimental verification is carried out to prove that the ultrasonic excitation signal generated by the transmitting system has small noise and steep waveform, which fully meets the engineering needs and has high accuracy and stability.

1. Introduction

Ultrasound is a kind of sound wave whose frequency is higher than 20,000 Hz. It has the characteristics of good direction, high power, strong penetration, easy to obtain concentrated sound energy, and no damage to the detected substances and human body[1-4].These advantages make ultrasound widely used in medical[5], military[6], agricultural[7] and almost all industrial flaw detection fields[8, 9]. In addition, ultrasonic detection has a lot of in-depth research and application in thickness measurement[10, 11], ranging and medical ultrasound imaging[12-14].For example, the bedding structure of shale can be detected by the response analysis of the ultrasonic characteristics, and the defects in the body welding can be monitored by the ultrasonic to ensure the safety of production;Some scholars apply the ultrasonic transmission method to the foundation pile detection, which can find the defects of the foundation pile in time and solve the potential safety hazards;and can also use the ultrasonic to detect the leakage of oil and gas wells or water injection wells or casing annulus leakage[15].

With the development of modern signal processing technology, the application field of ultrasonic flaw detection is expanding. However, in many applications, the parameters of the ultrasonic transmitting system require that the transmitting frequency and amplitude be precisely adjustable[16-18].At the same time, with the development of intelligent digital instruments, the new requirements of ultrasonic nondestructive testing, such as easy to carry, easy to store and analyze test data, are proposed[19, 20].herefore, in this paper, we use STM32 as the main control system to digitalize the parameters control and information processing and display of the launching system. At the same time, based on the analysis of the resistance and capacitance parameters of the launching system, we optimize the design parameters so that the parameters of the whole launching system

Copyright © (2018) Francis Academic Press, UK DOI: 10.25236/icscbd.2018.032

can be precisely adjusted.The system designed in this paper can also be combined with the existing ultrasonic scanning device of the laboratory to carry out measurement experiments of acoustic parameters under various conditions.

2. The overall design of the ultrasonic transmitting circuit

The whole circuit of non-metallic ultrasonic transmitting circuit is shown in Figure 1. The whole system consists of four parts: ARM main control system, DC power supply module, multi-channel module and pulse excitation circuit.The main control system uses the ARM chip STM32F1, which makes the whole system more functional. The specific design is shown in Figure 2.The main control chip of ARM not only controls the transmitting control of the transmitting circuit, but also lays a solid foundation for the future expansion of the whole system.Multichannel module can make single ARM chip drive multiple probes to transmit, which makes the measurement accuracy high, the speed fast and the programming simple. This mode is especially suitable for driving the ultrasonic emission matrix, which can enhance the detection efficiency and make the detection effect better.After the main control chip of ARM passes through the multi-channel module, it uses the DC high voltage module to provide stable DC high voltage. At the same time, it controls the switching control elements of the pulse excitation circuit to make the transmitting circuit generate high voltage pulse to load on the probe.The ultrasonic wave emitted by the probe can be used for flaw detection. Ultrasound transmitting circuit is an important part of the ultrasonic flaw detector. The accuracy and stability of this part are very important to the whole ultrasonic flaw detection system.

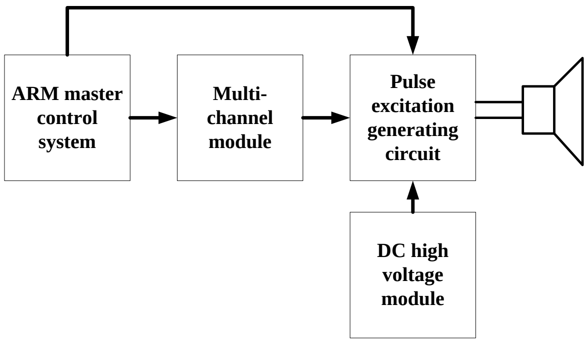

Figure 1 Overall Block Diagram of System

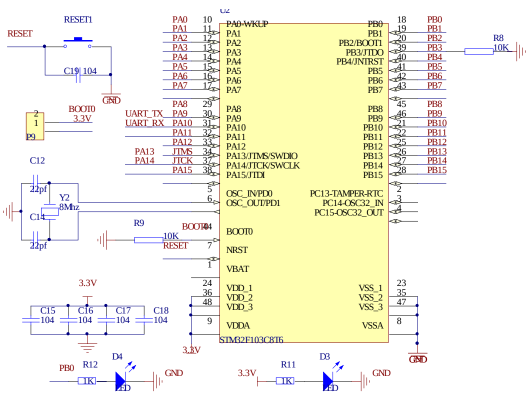

Figure 2 Design of ARM Main Control System

3. Design of Pulse Excitation Generator Circuit

The excitation signal generated by the microcontroller STM32F1 is a pulse signal which is applied to the excitation circuit to generate a high voltage spike. When the sharp pulse is suddenly applied to the piezoelectric crystal in the probe, the crystal produces high frequency vibration and emits a certain frequency of ultrasound due to the inverse piezoelectric effect of the piezoelectric crystal. The specific design is shown in Figure 3. When the output pulse of STM32F1 pin PA8 is in low level state, Q1 is cut-off state. At this time, the power supply charges capacitor C5 through R2, R3, R18, R19 and R5, and finally reaches the input DC power supply voltage of 500V.When the pulse output from the pin PA8 of the STM32F1 is in a high state, Q1 is turned on. At this time, the voltage across the capacitor C5 cannot be instantaneously changed. Therefore, the voltage of R5 is instantaneously pulled down to -500V. Finally, capacitor C5 is discharged through the turned-on MOS transistor Q1, resistors R5 and R6, and there is an excitation high voltage across R6. Resistors R2, R3, R18 and R19 are connected in the way shown in Fig. 3 to reduce the heat generated by the resistance and make the whole system run safely and steadily.

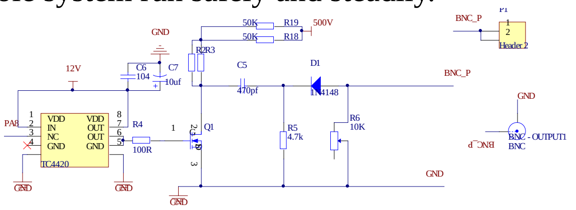

Figure 3 Pulse Excitation Generator Circuit

TC4220 is a high-speed MOSFET driver chip with a peak value of 6A. It is a phase driver.TC4220 is used to drive the MOS Q1.For a MOS transistor, the shorter the time it takes to pull the voltage between GS from zero to the opening voltage of the transistor, the faster the MOS transistor will open. Similarly, the shorter the time to drop the GS voltage of the MOS transistor from the open voltage to 0V, the faster the shutdown speed of the MOS transistor will be. In order to pull the GS voltage high or low in a shorter time, it is necessary to give the MOS tube gate a larger instantaneous driving current. The chip TC4220 is to provide a large drive current to the MOS transistor. Then there are the following requirements for the selection of MOS tube Q1:

①Since the DC power supply voltage HV ranges from 0V to 1000V, it is required $V_{DS} \geq 1000V$;

②The on-resistance should be small, only the resistance value of the switching device is very small, and the instantaneous discharge voltage is similar to the DC high voltage;

③Fast switching time.

Based on the above three points, the choice of this paper is IRFPG40, its $V_{DS} = 1000V$, $R_{DS(\mathrm{on})} = 3.5\Omega$, conduction delay time and turn-off delay time are all in the ns level.

4. Analysis of Resistance Capacitance Parameters of Ultrasonic Transmitting Circuit

When analyzing the charging and discharging of the charging and discharging transmitting circuit, we can equate the MOS transistor IRFPG40 with an ideal switch and resistance R4 in series. The diode D1 shown in Figure 2 can be equivalent to a resistor R3 in the discharge circuit, as shown in Figure 4.

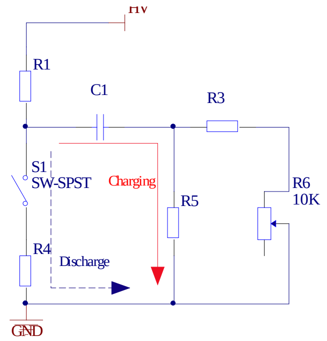

Figure 4 Equivalent Circuit Diagram of Ultrasound Transmitting Circuit

First, the discharge process is analyzed. During the discharge process, the MOS transistor is turned on, and the switch of Fig. 4 is closed. At this time, according to Kirchhoff's voltage law, we can obtain Equation 1:

$$\frac{R_4}{R_1 + R_4} V_H + i_c R_4 + i_c R_6 = U_c \tag{1}$$

Among them, V_H is the amplitude of DC high voltage power supply, U_c and i_c are the voltages and currents of capacitors respectively. At the same time, the current of the discharge circuit is:

$$i_c = -C_1 \frac{dU_C}{dt} \tag{2}$$

Bringing Equation 2 into Equation 1 gives you:

$$U_c + C_1(R_4 + R_6)\frac{dU_C}{dt} = \frac{R_4}{R_1 + R_4} V_H \tag{3}$$

Let $\tau = C_1(R_4 + R_6)$ and $u = \frac{R_4}{R_1 + R_4} V_H$, then Equation 3 can be reduced to:

$$\frac{dU_C}{dt} + \frac{1}{\tau} U_c = \frac{1}{\tau} u \tag{4}$$

Solution 4 can be obtained as follows:

$$U_c = u + C_0 e^{-\frac{t}{\tau}} \tag{5}$$

At the same time, according to the initial discharge $U_c = V_H$, we can get:

$$C_0 = \frac{R_1}{R_1 + R_4} V_H \tag{6}$$

So you can get it:

$$U_c = u + \frac{R_1}{R_1 + R_4} V_H e^{-\frac{t}{\tau}} \tag{7}$$

$$i_c = -C_1 \frac{dU_C}{dt} = \frac{R_1}{R_1 + R_4} V_H \frac{1}{R_4 + R_6} e^{-\frac{t}{C_1(R_4+R_6)}} \tag{8}$$

Then we can get the emission voltage at both ends of the probe as follows:

$$U_A = -\frac{R_1 R_6}{R_1 + R_4} V_H \frac{1}{R_4 + R_6} e^{-\frac{t}{C_1(R_4+R_6)}} \tag{9}$$

Then by analyzing the charging circuit again, we can also get the voltage equation of the charging circuit as follows:

$$V_H = i(R_1 + R_5) + U_c \tag{10}$$

Similarly, by substituting $i_c = C_1 \frac{dU_C}{dt}$ into Equation 10, we can get:

$$C_1(R_1 + R_5)\frac{dU_C}{dt} + U_c = V_H \tag{11}$$

Let $C_1(R_1 + R_5) = \tau_1$ be able to solve the differential equation of Equation 11 as:

$$U_c = V_H + C_2 e^{-\frac{t}{\tau_1}} \tag{12}$$

Similarly, according to the initial charging time $U_c = \frac{R_4}{R_1 + R_4} V_H$:

$$C_2 = -\frac{R_1}{R_1 + R_4} V_H \tag{13}$$

It can be:

$$U_c = (1 - \frac{R_1}{R_1 + R_4} e^{-\frac{t}{\tau_1}}) V_H \tag{14}$$

$$i_c = C_1 \frac{dU_C}{dt} = \frac{R_1}{R_1 + R_4} V_H \frac{1}{R_5 + R_1} e^{-\frac{t}{C_1(R_1+R_5)}} \tag{15}$$

Similarly, the instantaneous voltage value at charging time can be obtained as follows:

$$U_B = \frac{R_1 R_5}{R_1 + R_4} V_H \frac{1}{R_5 + R_1} e^{-\frac{t}{C_1(R_1+R_5)}} \tag{16}$$

(1)The Effect of Equivalent Resistance of Switch Tube

We calculate the parameters in Fig. 2, and we can get the results: $R_1 = 50K\Omega$, $R_4 = 3.5\Omega$, $R_6 = 10K\Omega$.According to formula 9, the instantaneous emission voltage can be calculated to be -499.8V.If the other parameters remain unchanged, we increase the equivalent resistance of the switch to 100 ohms, and the instantaneous emission voltage is about -494.06V.It can be seen from this that only when the equivalent resistance of the switch tube is small enough, the instantaneous discharge voltage is close to the magnitude of the DC high-voltage power supply. If the equivalent resistance of the switch becomes larger, the corresponding emission voltage will gradually decrease, affecting the emission effect. However, the circuit designed in this paper has minimized the influence of the equivalent resistance of the switching transistor. Usually the equivalent resistance of the switching MOS transistor is about several ohms, so the whole design increases the stability and compatibility of the whole system.

(2)Effect of resistance R1

Resistance R1 is designed to prevent the high voltage power supply from burning down due to excessive current during charging, so we call it current limiting resistance.R1can be seen according to Equations 9 and 16, which affect the instantaneous charging and instantaneous discharge voltage both. Increasing R1 will increase the instantaneous discharge voltage. Therefore, from the perspective of transmitting power, the greater resistance R1 is, and the higher transmitting power is, the deeper the flaw detection is. At the same time, it should be noted that if R1 reaches a certain level, the effect of increasing the instantaneous discharge voltage will be reduced. If R1 is large enough, it will make the charging time longer, affect the charge accumulation on both sides of the capacitor, and the charging time is too long, then the energy of capacitor accumulation will be lower in a certain period of time. At this time, too large R1 will reduce the instantaneous discharge voltage. Then the value of resistance R1 needs to take an appropriate value, usually tens of thousands of ohms.

(3)The Effect of Capacitance C1 and Resistance R6

In Equations 9 and 16, the capacitor C1 and the resistor R6 together affect the parameters of the excitation pulse. The smaller the capacitor C1 is, the shorter the discharge time of the capacitor charge and the smaller the pulse width and rise time of the excitation pulse, which will increase the longitudinal resolution and sensitivity of the entire system. But if the capacitance is too low, the stability of the whole system will be worse, and the amplitude of the excitation pulse generated is very unstable. Moreover, because the capacitance is small, the energy stored in the system during charging will be less, so the instantaneous discharge voltage will be too low, affecting the transmission power, so the value of the capacitance should be carefully chosen. Similarly, resistance R6 and capacitance C1 together affect the discharge time constant. The larger the R6, the larger the discharge time constant, the wider the excitation pulse and the lower the detection resolution. However, the larger the R6, the larger the instantaneous discharge voltage, but the effect of this increase is not obvious. Similarly, resistance R6 can also adjust the length of the pulse ultrasonic wave and play a damping role, so resistance R6 is also called damping resistance. Therefore, resistance R6 can be summarized as small resistance, then large damping, when the emission pulse is narrow, detection resolution is higher, but the transmission power is smaller; The bigger the resistance R6 is, the wider the pulse width and lower the detection resolution, but the transmitting power will be increased appropriately. In this paper, we set resistance R6 as variable resistance, which can adjust the emission intensity and pulse width according to the working conditions of the system.

5. Design of DC High Voltage Power Supply Module

DC power supply voltage HV uses Dongwen high voltage power supply module, input voltage 12V, output voltage 0-1000V adjustable. There are two ways of regulation: potentiometer regulation and external voltage regulation. In order to ensure the accuracy of regulation, potentiometer regulation is adopted here. As shown in Figure 5.The output voltage of the high voltage power supply module is adjusted by the resistance value of the digital potentiometer X9312. X9312 is a resistor array with 99 resistor units.The position of sliding end of digital potentiometer X9312 is changed by controlling the pins PA3, PA4 and PA5 of STM32F1 to realize the function of voltage dividing. The output voltage of HVDC power supply is adjusted by this voltage divider. The adjustable precision is about 20-30V. As shown in Figure 6.

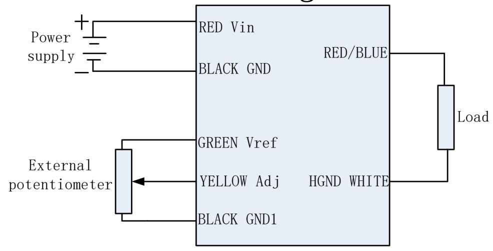

Figure 5 Connection Schematic Diagram of Potentiometer Regulation Mode

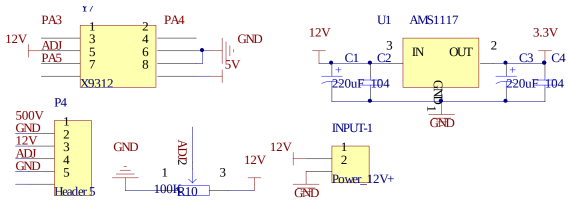

Figure 6 Auxiliary Module for DC High Voltage Power Supply

6. Experimental test

After theoretically designing the circuit, we used PROTEL to simulate the entire circuit design into a compact printed circuit board, which was then fabricated into a physical object, as shown in

Figure 7.Then we tested the circuit. The output pulse frequency of STM32F1 pin PA8 is 25KHz, duty cycle is 5%. That is, the period is 40us, and the high level lasts 2us.The duty cycle should not be changed, that is, the amplitude of output spike should not be adjusted by duty cycle, but by HV of HVDC power supply. Because when the output pulse of PA8 is in the low level state, Q1 is in the cut-off state, forming the RC charging circuit. But when the output pulse of PA8 is at high level, Q1 is connected. At this time, the input DC power supply voltage HV is grounded by R1 and R2. If the pulse is at high level for a longer time, the heat of R1 and R2 will increase. It makes the whole system unstable and even causes potential safety hazards. At this time, R1 = 50k, R4 = 3.5, R6 = 10K, and the theoretical value of our instantaneous emission voltage calculated by formula 9 should be -599.7V.From figure 8, we can see that the real value is -600V.And we adjust the DC high voltage power supply output 530V, and adjust the sliding rheostat to 1KΩ. According to Equation 9, we can calculate the theoretical value of the instantaneous emission voltage should be -528.1V, then the actual value is -528V.The correctness of the derivation of formula 9 and formula 16 can be fully proved by the above two experimental results. In addition, it can be seen from Figure 8 that the rise time and pulse width of the excitation pulse emitted by the system are several nanoseconds, which are fully qualified for engineering requirements. At the same time, the whole system has the advantages of high detection resolution and high transmission power.

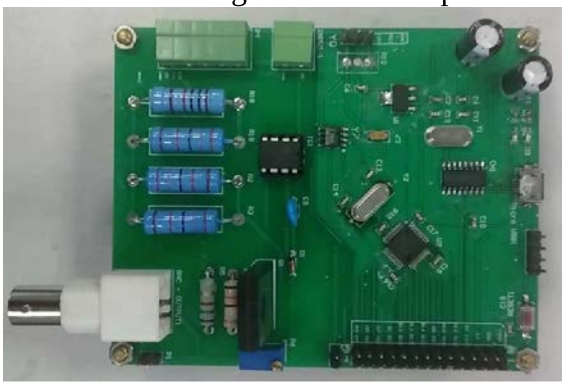

Figure 7 Physical Map of the Launch System

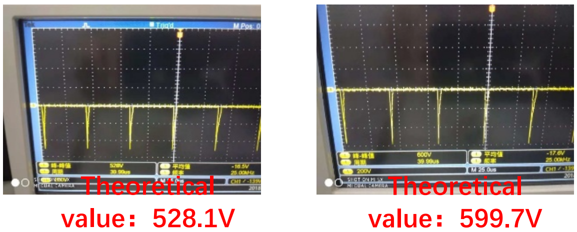

Figure 7 Comparison of Real and Theoretical Values

7. Conclusion

In this paper, a new type of capacitive instantaneous nonmetallic ultrasonic transmitting system is proposed.Firstly, the overall design block diagram of the system is presented. Then, based on the analysis of the resistance and capacitance parameters of the transmitting system, the voltage formula during charging and discharging is deduced theoretically. According to the deduced results, the influence of the resistance and capacitance of the capacitance instantaneous method on the transmitting system is discussed in detail. Then we optimize the parameters of the launching system on this basis. At last, the validity of theoretical deduction is proved by physical manufacture and experimental test, which provides a strong theoretical guidance for the design of the transmitting circuit of ultrasonic flaw detection in the future. At the same time, we also prove that the transmitting system designed in this paper has many advantages, such as multi-channel, precise adjustable transmitting parameters, high detection resolution and high transmitting power. The research of this paper can provide technical support and theoretical guidance for ultrasonic nondestructive testing, and has great practical value.

This work was supported by Dongguan Municipal Science and Technology Bureau under grant No. 2016508140.

References

[1] Olofsson, K., B. Hammarstrom and M. Wiklund, Ultrasonic Based Tissue Modelling and Engineering. Micromachines (Basel), 2018. 9(11).

[2] Simola, N. and S. Granon, Ultrasonic vocalizations as a tool in studying emotional states in rodent models of social behavior and brain disease. Neuropharmacology, 2018.

[3] Potasiewicz, A., M. Holuj, D. Piotrowska, K. Zajda, M. Wojcik, P. Popik, and A. Nikiforuk, Evaluation of ultrasonic vocalizations in a neurodevelopmental model of schizophrenia during the early life stages of rats. Neuropharmacology, 2018.

[4] Abbas, M. and M. Shafiee, Structural Health Monitoring (SHM) and Determination of Surface Defects in Large Metallic Structures using Ultrasonic Guided Waves. Sensors (Basel), 2018. 18(11).

[5] Kohlberg, G.D., N. Lipschitz, K.O. Tawfik, Z. Walters, J.T. Breen, M. Zuccarello, N. Andaluz, V.A. Dinapoli, M.L. Pensak, and R.N. Samy, Application of Ultrasonic Bone Aspirator for Decompression of the Internal Auditory Canal via the Middle Cranial Fossa Approach. Otol Neurotol, 2018.

[6] Zhang, H., G.Y. Chen, L. Xiao, X. Ma, L. Shi, T. Wang, H.T. Yan, H. Zou, Q. Chen, L.J. Tang, and W.H. Liu, Ultrasonic/CT image fusion guidance facilitating percutaneous catheter drainage in treatment of acute pancreatitis complicated with infected walled-off necrosis. Pancreatology, 2018. 18(6): p. 635-641.

[7] Wang, Y., X. Zhang, X. Ma, K. Zhang, S. Li, X. Wang, X. Liu, J. Liu, W. Fan, Y. Li, Q. Li, and X. Zhu, Study on the kinetic model, thermodynamic and physicochemical properties of Glycyrrhiza polysaccharide by ultrasonic assisted extraction. Ultrason Sonochem, 2018.

[8] Nguyen, L.T., G.K. Kocur and E.H. Saenger, Defect mapping in pipes by ultrasonic wavefield cross-correlation: A synthetic verification. Ultrasonics, 2018. 90: p. 153-165.

[9] Song, Y., J.A. Turner, Z. Peng, C. Chao, and X. Li, Enhanced Ultrasonic Flaw Detection using an Ultra-high Gain and Time-dependent Threshold. IEEE Trans Ultrason Ferroelectr Freq Control, 2018.

[10] Eto, Y., [Basic Evaluation of the Acoustic Lens Narrow Aperture Method Devised for Improving Elevational Resolution of Ultrasonic Probe]. Nihon Hoshasen Gijutsu Gakkai Zasshi, 2018. 74(10): p. 1170-1179.

[11] Wang, Y., M. Lian, H. Liu, Y. Ying, and L. Zhou, Incident Angle Identification Based on First-Echo Energy Attenuation in Ultrasonic Thickness Measurement. IEEE Trans Ultrason Ferroelectr Freq Control, 2018. 65(11): p. 2141-2149.

[12] Ye, J., S. Ito and N. Toyama, Computerized Ultrasonic Imaging Inspection: From Shallow to Deep Learning. Sensors (Basel), 2018. 18(11).

[13] Han, Y., C. Zhang, J. Pang, S. Wang, L. Zhang, K. Li, and B. Song, Qualitative diagnosis of benign breast lesions and breast carcinoma with elastographic ultrasonic imaging. J BUON, 2018. 23(4): p. 919-924.

[14] Imbault, M., B.M. Dioguardi, A. Faccinetto, M. Ronot, H. Bendjador, T. Deffieux, E.O. Triquet, P.E. Rautou, L. Castera, J.L. Gennisson, V. Vilgrain, and M. Tanter, Ultrasonic fat fraction quantification using in vivo adaptive sound speed estimation. Phys Med Biol, 2018. 63(21): p. 215013.

[15] Zhang, G., J. Zhu, Y. Song, C. Peng, and G. Song, A Time Reversal Based Pipeline Leakage Localization Method With the Adjustable Resolution. IEEE Access, 2018. 6: p. 26993-27000.

[16] Nguyen, L.T., G.K. Kocur and E.H. Saenger, Defect mapping in pipes by ultrasonic wavefield cross-correlation: A synthetic verification. Ultrasonics, 2018. 90: p. 153-165.

[17] Delrue, S., M. Tabatabaeipour, J. Hettler, and K. Van Den Abeele, Applying a nonlinear, pitch-catch, ultrasonic technique for the detection of kissing bonds in friction stir welds. Ultrasonics, 2016. 68: p. 71-9.

[18] Fendt, K.T., H. Mooshofer, S.J. Rupitsch, and H. Ermert, Ultrasonic Defect Characterization in Heavy Rotor Forgings by Means of the Synthetic Aperture Focusing Technique and Optimization Methods. IEEE Trans Ultrason Ferroelectr Freq Control, 2016. 63(6): p. 874-85.

[19] Liu, J., J. Han, H. Lv, and B. Li, An ultrasonic sensor system based on a two-dimensional state method for highway vehicle violation detection applications. Sensors (Basel), 2015. 15(4): p. 9000-21.

[20] Chen, C., Y. Wang, J. Yu, Z. Zhou, L. Shen, and Y.Q. Chen, Automatic motion analysis system for pyloric flow in ultrasonic videos. IEEE J Biomed Health Inform, 2014. 18(1): p. 130-8.